



OPEN

Differential toxicity profile of secreted and processed α -Klotho expression over mineral metabolism and bone microstructure

Joan Roig-Soriano¹, Cristina Sánchez-de-Diego², Jon Esandi-Jauregui¹, Sergi Verdés¹, Carmela R. Abraham³, Assumpció Bosch^{1,4,5}, Francesc Ventura² & Miguel Chillón^{1,4,6,7}✉

The aging-protective gene α -Klotho (KL) produces two main transcripts. The full-length mRNA generates a transmembrane protein that after proteolytic ectodomain shedding can be detected in serum as processed Klotho (p-KL), and a shorter transcript which codes for a putatively secreted protein (s-KL). Both isoforms exhibit potent pleiotropic beneficial properties, although previous reports showed negative side effects on mineral homeostasis after increasing p-KL concentration exogenously. Here, we expressed independently both isoforms using gene transfer vectors, to assess s-KL effects on mineral metabolism. While mice treated with p-KL presented altered expression of several kidney ion channels, as well as altered levels of P_i and Ca²⁺ in blood, s-KL treated mice had levels comparable to Null-treated control mice. Besides, bone gene expression of *Fgf23* showed a fourfold increase after p-KL treatment, effects not observed with the s-KL isoform. Similarly, bone microstructure parameters of p-KL-treated mice were significantly worse than in control animals, while this was not observed for s-KL, which showed an unexpected increase in trabecular thickness and cortical mineral density. As a conclusion, s-KL (but not p-KL) is a safe therapeutic strategy to exploit KL anti-aging protective effects, presenting no apparent negative effects over mineral metabolism and bone microstructure.

α -Klotho (KL) was discovered by Kuro-o et al. when studying a mouse strain that presented with a phenotype resembling accelerated human senescence¹. This strain was characterized by a mutation in the regulatory region of the KL gene and generated a strong reduction of the Klotho protein production. Since then, several functions have been described for KL, being currently considered as a pleiotropic anti-aging hormone.

Klotho gene is mainly expressed in the kidney and in the brain choroid plexus, and it encodes for two transcripts². The full length (m-KL) generates a type I transmembrane protein presenting two homologous extracellular domains, KL1 and KL2. The extracellular portion can be shed by proteolytic cleavage, generating processed KL (p-KL), also known as soluble KL, containing both KL1 + KL2 domains. Additionally, the KL1 and KL2 domains, can be shed generating independent soluble subunits³. Alternatively, a second transcript generates a shorter mRNA which presents a stop codon short after the KL1 domain, generating a secreted isoform (s-KL)². Although recent reports doubt if this endogenous transcript produces a functional protein⁴, different groups have reported that increasing the levels of s-KL or KL1 through recombinant protein administration or gene transfer approaches confers clear beneficial properties^{5–8}. Klotho can modulate several pathways related to aging progression, which include among others, the inhibition of insulin growth factor-1 (IGF-1)/insulin signaling

¹Department of Biochemistry and Molecular Biology, Institut de Neurociències (INc), Universitat Autònoma Barcelona, Bellaterra, Spain. ²Departament de Ciències Fisiològiques, Facultat de Medicina i Ciències de la Salut, IDIBELL, Universitat de Barcelona, L'Hospitalet de Llobregat, Spain. ³Departments of Biochemistry and Pharmacology & Experimental Therapeutics, Boston University School of Medicine, Boston, MA, USA. ⁴Vall d'Hebron Institut de Recerca (VHIR), Barcelona, Spain. ⁵Centro de Investigación Biomédica en Red Sobre Enfermedades Neurodegenerativas (CIBERNED), Instituto de Salud Carlos III, Madrid, Spain. ⁶Unitat Producció de Vectors (UPV), Universitat Autònoma Barcelona, Bellaterra, Spain. ⁷Institució Catalana de Recerca i Estudis Avançats (ICREA), Barcelona, Spain. ✉email: Miguel.Chillon@uab.es

and Wnt pathways, involved in senescence and fibrosis, respectively⁹. It also reduces oxidative stress and exhibits anti-inflammatory effects, reducing cellular damage during aging¹⁰. Besides, KL also plays a key role in mineral metabolism, where it is involved in direct modulation of ion channels, PTH hormone production, vitamin D regulation and fibroblast growth factor 23 (FGF23) hormone signaling¹¹. For more details on KL anti-aging functions, see the review by Abraham and Li, 2022¹².

Klotho has a direct impact over some ion transporter proteins increasing abundance and activity of these channels. Transient receptor potential cation channel subfamily V members 5 and 6 (TRPV5/6) calcium channels, potassium transporter renal outer medullary potassium channel 1 (ROMK1 or KCNJ1) and NaPi-2a cotransporter (SLC34A1), are activated and stabilized in the membrane by KL's sialidase activity^{13,14}. Moreover, KL is also involved in Na⁺, K⁺-ATPase channel transport to the membrane, responsible of Ca²⁺ reabsorption in the kidney¹³. Modulation of these channels represents a fast system of controlling ion concentrations.

In addition to this direct effect on ion transporters, KL also participates in metabolism of vitamin D (1,25D), which is responsible for increasing renal and intestinal absorption of Ca²⁺ and inorganic phosphate (P_i)¹⁵. In turn, activation of vitamin D receptor (VDR) by 1,25D upregulates Klotho transcripts and FGF23 production¹⁶, which will inhibit further 1,25D synthesis, promoting a decrease of P_i levels¹⁵.

Finally, KL is also implicated in FGF23 production and signaling pathway. FGF23 is a bone-derived hormone important for phosphate concentration regulation¹¹. After phosphate intake, FGF23 is secreted from osteocytes in the bones and reduces this ion concentration by different mechanisms. First, it increases renal phosphate excretion by downregulating NaPi-2a and NaPi2c (SLC34A3) ion channels. Secondly, it inhibits vitamin D activation, downregulating renal 1- α -hydroxylase (CYP27B1) and promoting vitamin D degradation by increasing 24-hydroxylase (CYP24A1) enzyme¹⁷.

Klotho implication in FGF23 signaling was well known from the study of the phenotypes of the *klotho* knock out (KO) mice and the *Fgf23* KO mice. Both mutants presented hyperphosphatemia, increased vitamin 1,25D, ectopic calcifications, and extremely shortened lifespan^{1,18,19}. In contrast, just Klotho overexpression increased lifespan, suggesting FGF23 is not related to this Klotho property^{20,21}. In this system, transmembrane KL (m-KL) acts as an obligate co-receptor for FGF23 signaling. This is due to the interaction of Klotho with FGFR1, FGFR3 and FGFR4, receptor proteins responsible for FGF23 signaling. This interaction increases affinity of the FGF23 receptors for their FGF23 ligand, making possible the receptor activation. In a structural-molecular point of view, FGFR interacts with a region in KL2 domain, stabilizing the binding. Deletion of the receptor binding loop (RBL) region of KL2 inhibits Klotho-induced increase in phosphate urinary excretion, proving a decreased FGF23 activity¹¹. Importantly, Klotho also affects FGF23 production, as exogenous administration of p-KL (or soluble KL) induced a significant increase in the FGF23 amount in serum, altering mineral metabolism²².

The pleiotropic beneficial properties of KL protein isoforms represent a promising strategy to treat different age-related diseases. However, due to the key role in mineral homeostasis, exploiting protective anti-aging effects of p-KL could in turn translate in deregulation of the bone ion regulation system. Currently, it is unknown whether the s-KL isoform also promotes FGF23 production in osteocytes in vivo and present the same toxic effect observed for p-KL. Here, we aimed to address this question.

Results

Gene therapy treatment efficiently overexpresses secreted and processed KL isoforms. Expression cassettes under the control of the CMV promoter were cloned carrying Control-Null sequence (stuffer, non-coding sequence), secreted (s-KL), or processed KL (p-KL) sequences (Fig. 1a). Different adeno-associated viral vectors serotype 9 (AAV9) were generated for each construct and the animals were administered IV and ICV at the age of 3 months (Fig. 1b), without observed intervention-derived negative effects. Body weight increase at that age was not affected by the treatments as can be seen in the follow-up done during the 2 months-long treatment (Fig. 1c). As expected after an intravenous injection, AAV9 vectors efficiently increased viral vector expression in liver, similarly in male and female mice (Fig. 1d), which in turn led to increased levels of KL isoforms in serum (Fig. 1e). Both isoforms were increased compared to Null group levels, although secreted isoform displayed higher levels both in males and females, compared to the processed KL isoform. Of note, females presented higher basal KL levels compared to males treated with Null vector.

The secreted KL isoform does not alter ion metabolism in young C57BL/6J mice. Serum of treated animals was analyzed to study alterations in ion homeostasis. Eight weeks after vector administration, p-KL treated animals showed a decrease in phosphate (P_i) and calcium (Ca²⁺) ions concentration, reaching significant differences compared to control and s-KL treated animals (Fig. 2a). Also, as seen in Fig. 2b, only p-KL altered the expression of different ion channels. ROMK and sodium chloride cotransporter SLC12A3 (also known as NCC) were significantly increased, and the TRPV5 channel exhibited a trend both in males and females. In contrast, no changes were observed after s-KL treatment. Of note, no expression changes were observed for the *Fgfr* genes (data not shown).

Enzymes of Vitamin D metabolic pathway were also affected after treatment. In kidney, 25(OH)D, precursor for vitamin D, is either enzymatically activated (CYP27B) or inactivated (CYP24A). Interestingly, after AAV administration, males treated with p-KL presented an increase in the expression of the inactivating *Cyp24b* gene, while the vitamin D synthesis gene *Cyp27b*, was reduced. In contrast, females treated with s-KL presented a significant reduction in the expression of the vitamin D catalytic *Cyp24a* gene, compared to Null and p-KL animals. No changes were observed for *Cyp27b* gene in s-KL treated animals (Fig. 2c).

Effect of KL-expressing vectors in bones. Intravenous administration of AAV9 viral vectors also allowed transduction of the bone tissue, increasing more than 100-fold over basal expression of Klotho isoforms

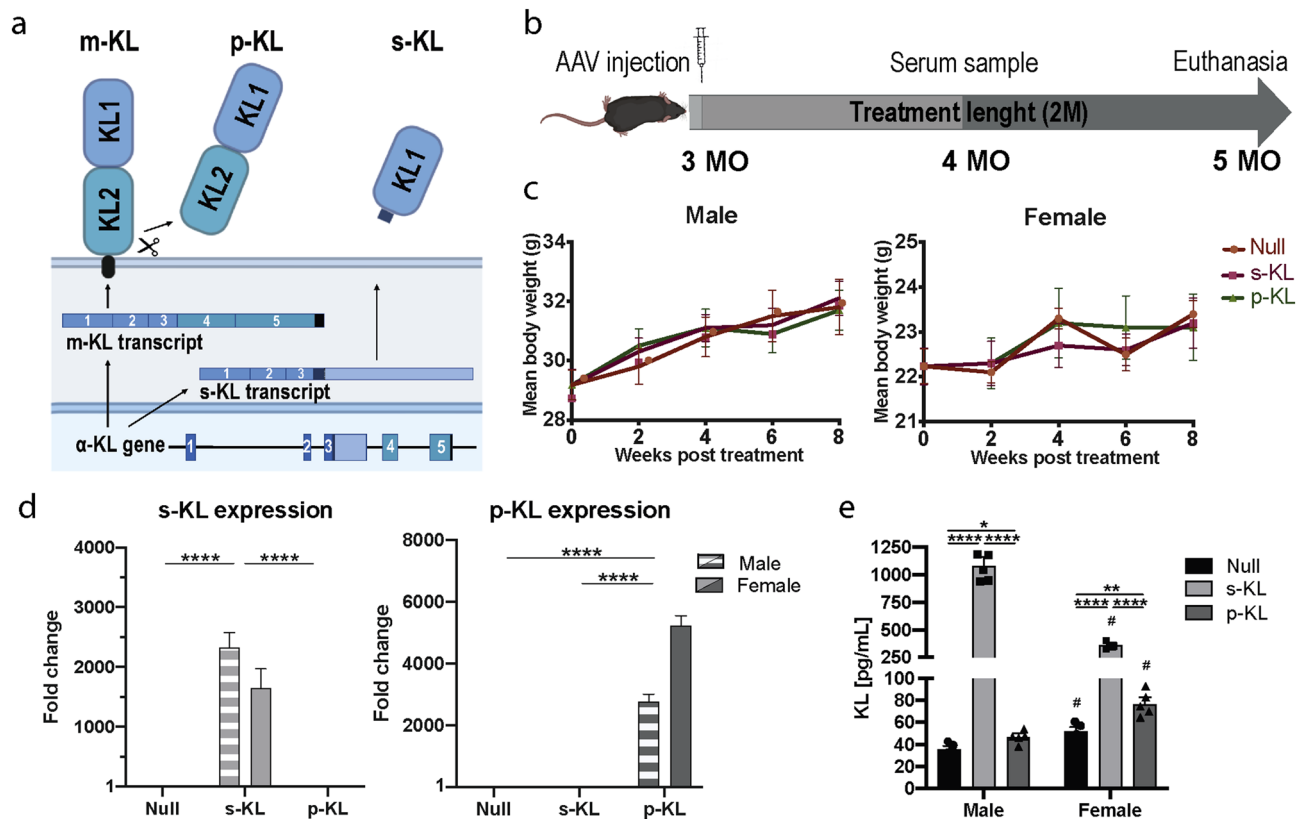


Figure 1. (a) Scheme with the different KL isoforms. (b) Experimental design followed. (c) Body weight follow up displayed as increase in grams during the 8 weeks-long treatment. No differences in body weight were observed between groups before the start of the experiment ($t=0$) or after 8 weeks. (d) Gene expression of secreted and processed KL in liver 2 months after the treatment. Stripped bars represent gene expression in males and solid bars in females. Data presented as fold change expression compared to Null treated animals. (e) KL protein levels in serum 2 months after the treatment. Mean \pm Standard error of the mean (SEM) for (c,e), and relative quantity (RQ) \pm standard error of RQ for (d); $n=4-6$; # $p<0.05$ for differences between males and females, * $p<0.05$; ** $p<0.01$; *** $p<0.001$; **** $p<0.001$ for differences between different treatment groups within the same gender.

in both sexes. No significant differences were observed in the overexpression between genders (Fig. 3a). *Fgf23* gene was strongly affected by the treatment. p-KL generated a four and six-fold increase in males and females, respectively. Interestingly, the secreted isoform s-KL did not alter *Fgf23* expression (Fig. 3b). In turn, both KL isoforms activated typical KL downstream signaling, with a tendency to decrease *c-Fos* expression in males, and increasing its expression in females, reaching significance for s-KL isoform (Fig. 3c).

The expression of different genes related to lineages of osteocytes (*Dmp1*), osteoblasts (*Sp7* and *Runx2*), osteoclasts (*Acp5* and *Ctsk*) and genes related to bone resorption *Tnfrsf11* (*RankL*) and *Tnfrsf11b* (*Opg*) were not statistically modified by the treatment (Fig. 3d), except for a significant reduction of *Dmp1* and the bone resorption protective protein OPG, in p-KL treated males. Expression of osteocalcin (*Bglap*), *Bmp2*, *Col1a1* and osteopontin (*Spp1*) genes, involved in bone structure was also assessed (Fig. 3e). A significant reduction in *Spp1* and a clear tendency to a reduced *Bglap* expression were observed in p-KL treated males, while no effects were observed in s-KL treated animals.

Klotho treatments affect differently bone structure and physical properties. The effects of overexpression of the different Klotho isoforms on bone microstructure was assessed by MicroCT analysis. Specifically, cortical bone, medullar cavity and trabecular bone parameters were measured. As observed in Fig. 4a, the p-KL isoform had a significant impact over cortical bone, reducing bone volume and cortical thickness by more than 10%, both in males and females. Interestingly, treatment with s-KL increased cortical mineral density (MD) compared to Null-treated mice. No changes were detected in bone length, perimeter or endocortical volume. As expected, males exhibited significantly higher levels of trabecular volume than females, even in the Control-Null group. In accordance with cortical bone, p-KL treatment in males also reduced trabecular bone volume (BV/TV), trabecular number and thickness, and increased trabecular spacing. Interestingly, the s-KL isoform did not induce this osteopenic phenotype and, in fact, even significantly increased the trabecular thickness compared to control mice (Fig. 4a). These structural differences can be seen in the 3D reconstruction of the ROI analyzed (Fig. 4b).

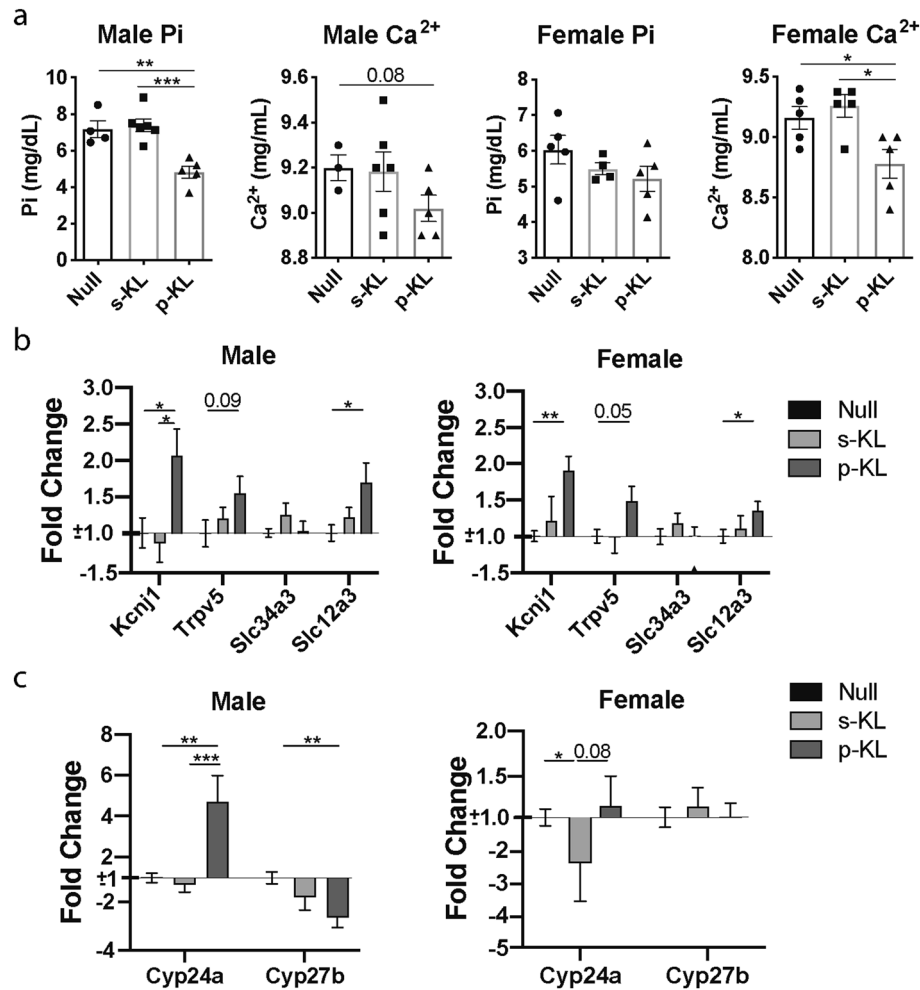


Figure 2. (a) Ca²⁺ and Pi serum levels after 8 weeks of treatment. (b) Expression of ion channels in kidney. (c) Expression of genes involved in vitamin 1,25D activation and degradation. Data are presented as fold change expression compared to Null-treated animals. Mean \pm Standard error of the mean (SEM) for (a), and relative quantity (RQ) \pm standard error of RQ for (b,c); n = 4–6; *p < 0.05; **p < 0.01; ***p < 0.001 for differences between the treatment groups.

Finally, a three-point bending test was done in order to assess the effect of these structural changes on bone physico-mechanical properties (Fig. 4c). Results showed that the p-KL treatment reduced the maximum load the bones could resist before starting to bend. Moreover, a reduction in load at fracture was also observed in males. In contrast, the s-KL treatment did not reduce neither maximum load, nor load at fracture, thus demonstrating a safer profile than the p-KL treatment. Lastly, s-KL and p-KL did not induce significant changes to stiffness, elasticity (displacement pre-fracture) and total energy absorption.

Discussion

Klotho isoforms are known as potent pleiotropic anti-aging proteins, which could be used as a treatment for different age-related conditions. However, its implication in mineral homeostasis requires special attention to avoid undesired deregulation of the ion balance.

After the eight weeks long treatment, AAV vectors efficiently expressed KL isoforms in the different tissues analyzed that translated into increased basal KL protein levels in serum of treated animals. Although p-KL gene expression in liver resulted in higher levels, s-KL isoform treatment generated significantly more protein in serum. The secreted isoform is shorter than processed KL, which could increase the translation and secretion rate of the protein, and explain the higher levels observed. Moreover, p-KL can interact with FGFR and could be partially retained in cell membranes. However, even though it reached lower protein levels, p-KL protein had a large impact in calcium (Ca²⁺) and phosphate (P_i) homeostasis, significantly decreasing their levels in serum. These results are in agreement with Smith et al., which described altered ion balance after p-KL expression²². In contrast, s-KL did not significantly alter ion levels, proving that the KL2 domain, found only in p-KL, is needed for this effect. To our knowledge, this is the first time this effect is described and compared for the s-KL and p-KL isoforms.

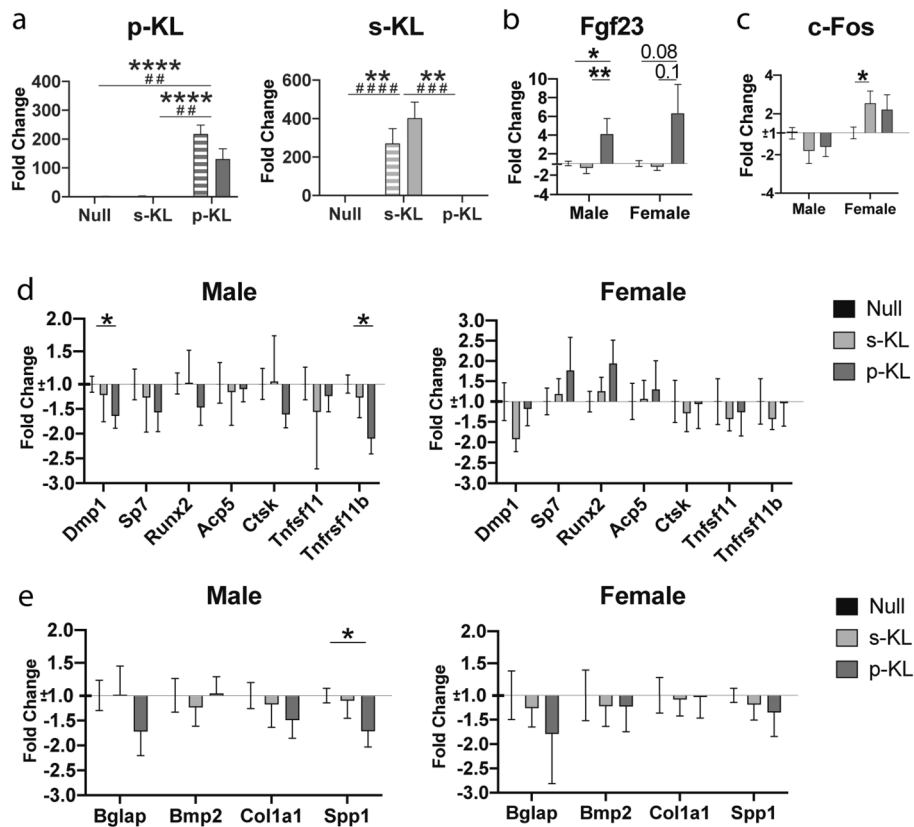


Figure 3. (a) Gene expression of secreted and processed KL in bone tissue 2 months after the treatment. Stripped bar represents gene expression in males and solid bar in females. Statistical significance presented as (*) for representing differences between treatment in male groups, and (#) for comparing treatments in females. (b) Effect of treatment on *Fgf23* gene expression. (c) Expression analysis of Klotho down-stream gene *c-Fos*. (d) Effect of treatment on cell type specific gene expression. (e) Effect of treatment on bone protein matrix gene expression. Data are presented as fold change expression compared to Null treated animals. Relative quantity (RQ) \pm standard error of RQ; n = 4–6; *p < 0.05; **p < 0.01; ***p < 0.001; ****p < 0.001 for differences between the treatment groups.

Activation of the FGFR/KL complex by FGF23 decreases phosphate levels by first reducing Na-dependent P channels and, secondly, by inhibiting vitamin D metabolism¹⁴. In this study, expression of *Slc34a3* channel (also known as *Npt2c*) did not change after upregulation of both KL isoforms. In contrast, KCNJ1 (ROMK channel), in charge of secreting potassium into the urine, was upregulated in p-KL-treated animals, which is in agreement with Cha and collaborators, who reported that KL administration increased KCNJ1 channels in distal nephrons in the kidney, increasing potassium secretion to urine²³. TRPV5 channel, which reabsorbs calcium in the kidney, also tended to increase in p-KL treated males and females. This effect could be a compensatory mechanism to recover decreased Ca²⁺ levels in p-KL animals. Additionally, NCC channel (SLC12A3), which participates in reabsorbing sodium and chloride ions from urine, was also upregulated. This was also observed in the KL-overexpressing transgenic mouse²⁴. Of note, ion channel alterations were not observed after the s-KL treatment suggesting no negative effects of this isoform on the kidney transporters studied here.

Secondly, enzymes related to vitamin 1,25D activation, responsible for increasing calcium and phosphate accumulation, were also studied in kidney. Vitamin D activator CYP27B and degrading CYP24A enzymes were significantly down and upregulated, respectively, after p-KL treatment in males. This result agrees with the observed reduced phosphate and calcium levels in blood. Again, s-KL had no effect over 1,25D metabolism. Interestingly, s-KL treatment in females decreased vitamin D degrading CYP24A enzyme, although this did not translate into higher ion levels compared to Null mice. More specific research is needed to understand the different effects of p-KL and s-KL isoforms that are gender-specific.

Based on the results obtained, we hypothesize that these alterations observed in FGF23 signaling are due merely to the increased FGF23 levels in p-KL treated mice, and not due to increased KL-dependent activity of the FGF23 receptor. Previous reports already provided evidence that p-KL increased FGF23 production, specifically by osteoblasts in bones. This generated hypophosphatemia and low 1,25D levels, provoking osteoporosis and osteomalacia²². This effect was independent of p-KL effect over KL/FGF23 signaling because, although p-KL can bind to FGFR, it is thought to not transduce intracellularly the FGF23 signal²⁴. This finding prompted us to try to address this effect with additional KL isoforms and subunits. To test whether the s-KL isoform affected or not *Fgf23* expression, we analyzed the expression of key genes in bones. In our model, p-KL overexpression

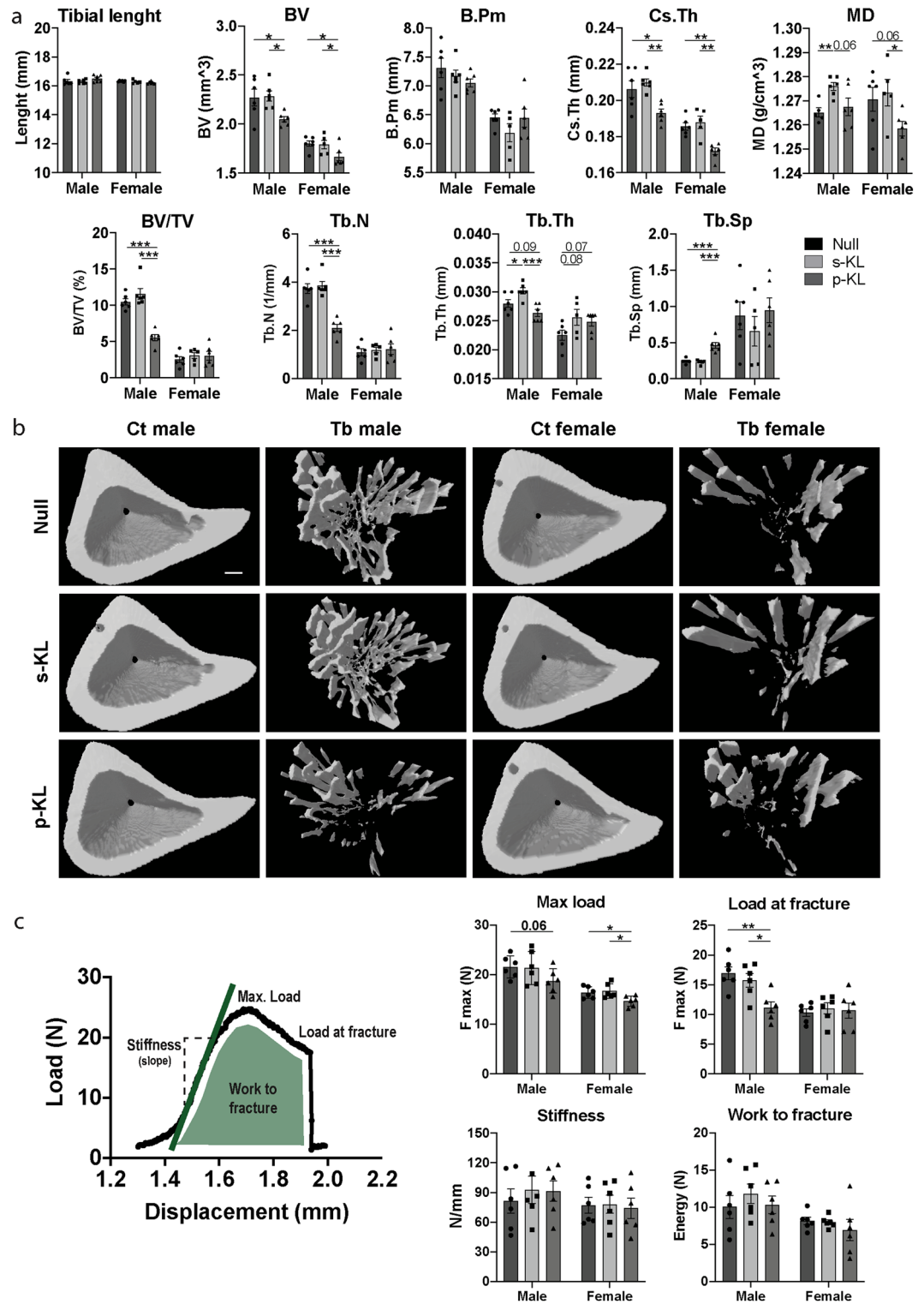


Figure 4. (a) MicroCT analysis of different structural variables. Tibial length, BV (bone volume), B.Pm (bone perimeter), Cs.Th (cross-sectional thickness), Mineral Density (MD), BV/TV (bone volume/tissue volume), Tb.N (trabecular number), Tb.Th (trabecular thickness), Tb.Sp (trabecular space). (b) 3D reconstruction of the analyzed ROI. First and third columns corresponding to cortical bone and second and fourth to trabecular bone. Scale bar = 0.2 mm. (c) Results of three-point bending test. Data represented as maximum load resisted by the bones, force at fracture, stiffness, and total energy absorbed by the bones during the experiment. Data are presented as fold change expression versus Null treated animals. Mean ± Standard error of the mean (SEM), n = 4–6; *p < 0.05; **p < 0.01; ***p < 0.001; ****p < 0.001 for differences between the treatment groups.

increased 4 times the *Fgf23* expression compared to control-Null mice. This result agrees with Smith et al., who described a FGF23 upregulation after a p-KL (soluble KL1 and KL2 domains) treatment²². Importantly, s-KL did not cause this increase in *Fgf23* expression, which could explain why s-KL does not produce a negative effect on mineral homeostasis. In turn, both isoforms were able to affect *c-Fos* expression, the downstream KL pathway, confirming both KL isoforms are functional, although only p-KL induces FGF23 upregulation. Klotho-mediated upregulation of *Fgf23* expression, was also observed in the KL-overexpressing mouse model, which also exhibits elevated FGF23 levels. Contrary, this mouse model did not present bone problems or phosphate dysregulation. This could be due to compensatory mechanisms present in the transgenic strain, like the observed reduction in 1,25D and parathyroid hormones and the regulation of phosphate channels expression²⁵.

We also tested the possible side effects of KL treatment over bone microstructure, by doing a microCT analysis of the long bone tibia. As previously described, p-KL treatment had a big osteopenic impact over bone mineral density and microstructure, in both cortical and trabecular bone²². Both genders presented similar effects, although females at a lower magnitude, which could be related to the lower trabecular bone mass, characteristic of female bones.

Interestingly, the s-KL treatment not only lacked negative side effects, but exhibited an improvement in bone status increasing bone mineral density and trabecular thickness in male mice. Previous reports from our group already described a possible positive effect of s-KL isoform over-expression in bones. Long bones of aged SAMP8 mice treated with s-KL AAVs presented microstructure values comparable to the healthy control SAMR1, while Null-vector treated mice presented values equivalent to aged SAMP8 mice⁵.

In addition, in p-KL treated males the effects over bone microstructure were accompanied by a reduction in expression of genes characteristic of osteocytes and bone resorption, and further accompanied by a decreased expression of osteopontin (*Spp1*) and osteocalcin genes (*Bglap*), both components of the bone structure. This finding together with the reduced ion availability could explain the observed alterations in the bones of p-KL-treated animals. Microstructure alterations caused by p-KL provoked a negative effect over bone tissue function. As observed, the p-KL treatment led to weaker bones, exhibiting decreased supported maximum load and load at fracture values, confirming specific negative side effects associated with high levels of this isoform.

Different previous studies had reported negative effects of exogenous KL administration over bone mineralization, discouraging its use as an anti-aging treatment²⁶. This effect was also described for humans, since a mutation leading to a strong increase of p-KL in serum also induced hypophosphatemia and hyperparathyroidism²⁷. On the other hand, several studies emphasize the importance and beneficial effects of Klotho for correct bone homeostasis, as knockout (KO) Klotho mice show important osteoporotic phenotype attributed to ion deregulation¹. Moreover, Klotho is involved in the correct expression of non-collagenous bone proteins and bone microstructure formation. As such, KO Klotho mice present altered BGLAP and DMP1 protein microstructure²⁸. Interestingly, the s-KL isoform has been reported to increase expression of these structural genes in in vitro osteoblast cultures²⁹. Although that effect was not reproduced in our in vivo experiment (Fig. 3e), we have detected improved trabecular and mineral density in bones of male mice treated with s-KL. RNA expression analysis of just osteoblasts could provide with more precise information to elucidate the mechanisms of improvement in those variables.

In summary, in this work, we have shown evidence that high s-KL levels do not induce the deleterious side effects of p-KL over ion balance and bone homeostasis, while high p-KL levels lead to a decrease in calcium and phosphate ions and alter expression of 25(OH)D, renal ion-transporters and channels. These changes led to reduced bone tissue and weaker bones. In contrast, s-KL did not alter those pathways and even improved some of the bone variables, although more research is needed to better understand the effect of s-KL over bone tissue microstructure. In conclusion, high levels of s-KL, but not p-KL, present a good biosafety profile, which facilitates its use as a long-term therapeutical molecule to treat aging-associated deficits.

Material and methods

Animal housing. C57BL/6J male (n=18) and female mice (n=18) were purchased from Charles River. These animals were randomly divided into 3 groups: Null control mice (n=6), s-KL (n=6) or p-KL (n=6) treated animals per sex. Mice had free access to food and water and were kept under standard temperature conditions (22 ± 2 °C) and a 12-h light/dark cycle (300 lx/0 lx). Gene therapy approach consisted in expression cassettes under the control of the CMV promoter containing secreted (s-KL) or processed (p-KL) isoforms of the mouse α -KL gene or a control-null sequence. Three adeno-associated viral vectors serotype 9 (AAV9), containing independently those constructs, were generated at the Unitat de Producció de Vectors (UPV) (www.viralvector.eu) following the triple transfection method³⁰. Animals were administered simultaneous by intracerebroventricular (ICV) and intravenous (IV) injection, to transduce as many tissues as possible. Intracerebroventricular stereotaxic injections of AAV vectors were performed as previously described⁵. Briefly, the treatment was administered into the right hemisphere at coordinates, -0.2 mm antero-posterior, -2 mm dorso-ventral, and +1 mm medio-lateral from bregma. The vector dose was 1×10^{11} viral genomes per animal in 6 μ l, administered at a 0.5 μ l/min speed using an ultramicropump (WorldPrecision Instruments). The intravenous injection consisted in a dose of 4×10^{11} viral genomes per animal diluted with NaCl 0.9% to a final volume of 200 μ l, and injected manually with a syringe into the lateral tail vein of the mice. After the two months long treatment, animals were deeply anaesthetized with 4–5% Isoflurane and sacrificed by decapitation, according to ethical procedures.

Serum biochemical analysis. Blood samples were obtained by decapitation, with a Serum Separation Tube (BD microtainer). Blood was left at room temperature for 5 min and then placed on ice. Blood serum was isolated by centrifugation at 3000 rpm for 15 min, and finally aliquoted and kept frozen at -80 °C. Calcium and

phosphate serum levels were measured at the Servei de Bioquímica Clínica Veterinària at the UAB, at 340 nm following the Arsenazo III and Phosphomolybdate methods, respectively. KL serum levels were measured using an ELISA kit specific for mouse KL (IBL) following manufacturer's indications.

Gene expression. Total RNA isolation was carried out using TRIsure™ reagent following the manufacturer's instructions (Bioline Reagent). The tissues used for the extraction were liver, half kidney, and long bones (tibia and femur without medulla). Tissues were homogenized using TissueLyser LT sample disruption apparatus (QIAGEN). RNA quantity and purity were measured with NanoDrop™ 1000 Spectrophotometer (Thermo Scientific). RNA retrotranscription was done using iScript™ Advanced cDNA Synthesis Kit (Bio-rad). Gene expression was analyzed by Real-Time quantitative PCR (RT-qPCR) on a Bio-Rad CFX-384 PCR machine at the Analysis and Photodocumentation Service of the Universitat Autònoma de Barcelona. Each reaction contained 25 ng of cDNA, 7.5 µl of iTaq™ Universal SYBR Green Supermix (Bio-Rad) and a primer concentration of 0.2 nM, with a final reaction volume of 15 µl. In case of TaqMan probes (ThermoFisher scientific), 5 µl of master mix (Norox), 0.5 µl TaqMan mix and H₂O to a final volume of 10 µl were used. Primers and TaqMan used are listed in Tables 1 and 2. The actin b (Actb) gene was used as a housekeeping control for qPCR done with SYBR green. The TATA binding protein (Tbp) gene was used as a housekeeping control for qPCR using Taqman done with RNA from bones, and Gapdh gene for Taqman qPCR done with RNA from the kidneys and liver. The analysis of the results of qPCR was done following the $\Delta\Delta C_t$ method. Briefly, the cycle threshold (C_q) value of each gene of interest was normalized by subtracting the difference of the housekeeping gene (HK) C_q of each sample with respect the HK's average value. Finally, data were presented as fold change in expression compared to Null-treated animals.

MicroCT. Bone microstructure study was done as previously described⁵. Briefly, right legs of perfused animals were isolated, fixed with PFA 4% solution and stored in PBS solution with 0.05% sodium azide (NaN₃). MicroCT analysis was done with a SkyScan 1272 (Bruker) computerized microtomography imaging system at the Centre de Recerca en Ciència i Enginyeria Multiescala de Barcelona (CRCEMB) at Universitat Politècnica de Catalunya (UPC). Images were reconstructed with the NRecon v1.6 (Bruker) program and analyzed with the

Target	Forward primer	Reverse primer
Cyp24a1	CTGCCCATTTGACAAAAGGC	CTCACCGTCGGTCATCAGC
Cyp27b1	GCACAGTTTACGTTGCCGAC	CGTTAGCAATCCGCAAGCA
s-KL	TCATAATGGAAACCTTAAAAGCAA	CAC TGGGTTTTGTCAAAGGA
p-KL	TACGGAGACCTCCCGATGTA	CGCAAAGTAGCCACAAAGGT
Actb	CAACGAGCGGTTCCGAT	GCCACAGGTTCCATACCCA

Table 1. Sequence of SYBR green primers used.

Target	Taqman reference
<i>Acp5</i>	Mm00475698_m1
<i>Bglap</i>	Mm03413826_mH
<i>Bmp2</i>	Mm01340178_m1
<i>c-Fos</i>	Mm00487425_m1
<i>Col1a1</i>	Mm00801666_g1
<i>Ctsk</i>	Mm00484039_m1
<i>Dmp1</i>	Mm01208363_m1
<i>Egr1</i>	Mm00656724_m1
<i>Fgf23</i>	Mm00445621_m1
<i>Gapdh</i>	Mm 99999915_g1
<i>Slc12a3 (NCC)</i>	Mm01173990_m1
<i>Slc34a3 (Npt2c)</i>	Mm00551746_m1
<i>Runx2</i>	Mm03003491_m1
<i>Kcnj1 (Romk)</i>	Mm01173990_m1
<i>Spp1 (Opn1)</i>	Mm00436767_m1
<i>Sp7 (Osx)</i>	Mm00504574_m1
<i>Tbp</i>	Mm00446973_m1
<i>Tnfrsf11 (RANKL)</i>	Mm00441906_m1
<i>Tnfrsf11b (Opg)</i>	Mm00435454_m1
<i>Trpv5</i>	Mm01166037_m1

Table 2. References of Taqman probes used.

CT-Analyser v1.13 image program (Bruker). Finally, 3D representations of the bones were obtained with the CTVox v3.3 program (Bruker). Mineral density was calculated with the CT-Analyser v1.13 program calibrating bone absorbance with two 2 mm diameter hydroxyapatite phantoms (Bruker-MicroCT) of known density of 0.25 and 0.75 g/cm³.

Three-point bending test. Bone resistance to fracture was measured by three-point bending test done at the Biomaterials, Biomechanics and Tissue Engineering Group, Technical University of Catalonia (UPC), Barcelona, Spain. A Bionix 358 servohydraulic mechanical testing machine (MTS Sensor Technologie GmbH & Co. KG, Lüdenschied, Germany) with a 500 N load cell was used for applying the force and recording the bone resistance to be deformed. All tibia samples were positioned with the same orientation and the same load velocity (1 mm/min) was applied for each test.

Statistical analysis. Statistical analysis and graphic representation were done with GraphPad Prism ver.8 (GraphPad Software). Statistical differences between groups were analyzed with a two-tailed unpaired Student's t-test when comparing two groups, one-way analysis of variance (ANOVA), followed by Tukey as a post-hoc analysis for comparing all treatment groups, and two-way ANOVA when the gender of the animal was considered. qPCR data are expressed as relative quantity of the gene of interest versus the reference genes \pm standard error of the relative quantity. All the other data are expressed as mean \pm standard error of the mean (SEM). Statistical difference was accepted when p values were ≤ 0.05 , and outliers were detected by Grubb's test and removed from the analysis.

Ethical approval. All experimental procedures involving animals were designed and performed following standard guidelines of the European Communities Council Directive 86/609/EEC and the ARRIVE guidelines. These were approved by the Institutional Animal Care and Use Committee of the Universitat Autònoma de Barcelona (M0348-DO5, approved procedure code, P1-4882) and biosecurity procedure HR-265-16.

Data availability

Data that support the findings of this study are available from the corresponding author upon reasonable request.

Received: 19 October 2022; Accepted: 7 March 2023

Published online: 14 March 2023

References

- Kuro-o, M. *et al.* Mutation of the mouse klotho gene leads to a syndrome resembling ageing. *Nature* **390**, 45–51. <https://doi.org/10.1038/36285> (1997).
- Shiraki-Iida, T. *et al.* Structure of the mouse klotho gene and its two transcripts encoding membrane and secreted protein. *FEBS Lett.* **424**, 6–10. [https://doi.org/10.1016/s0014-5793\(98\)00127-6](https://doi.org/10.1016/s0014-5793(98)00127-6) (1998).
- Chen, C. D. *et al.* Identification of cleavage sites leading to the shed form of the anti-aging protein klotho. *Biochemistry* **53**, 5579–5587. <https://doi.org/10.1021/bi500409n> (2014).
- Mencke, R. *et al.* Human alternative Klotho mRNA is a nonsense-mediated mRNA decay target inefficiently spliced in renal disease. *JCI Insight* **2**, 94375. <https://doi.org/10.1172/jci.insight.94375> (2017).
- Roig-Soriano, J. *et al.* AAV-mediated expression of secreted and transmembrane alphaKlotho isoforms rescues relevant aging hallmarks in senescent SAMP8 mice. *Aging Cell* **21**, e13581. <https://doi.org/10.1111/accel.13581> (2022).
- Masso, A., Sanchez, A., Bosch, A., Gimenez-Llort, L. & Chillón, M. Secreted alphaKlotho isoform protects against age-dependent memory deficits. *Mol. Psychiatry* **23**, 1937–1947. <https://doi.org/10.1038/mp.2017.211> (2018).
- Gupta, S. *et al.* KL1 domain of longevity factor Klotho mimics the metabolome of cognitive stimulation and enhances cognition in young and aging mice. *J. Neurosci.* **42**, 4016–4025. <https://doi.org/10.1523/JNEUROSCI.2458-21.2022> (2022).
- Abramovitz, L. *et al.* KL1 internal repeat mediates klotho tumor suppressor activities and inhibits bFGF and IGF-I signaling in pancreatic cancer. *Clin. Cancer Res.* **17**, 4254–4266. <https://doi.org/10.1158/1078-0432.CCR-10-2749> (2011).
- Moos, W. H. *et al.* Klotho pathways, myelination disorders, neurodegenerative diseases, and epigenetic drugs. *Biores. Open Access* **9**, 94–105. <https://doi.org/10.1089/biores.2020.0004> (2020).
- Yamamoto, M. *et al.* Regulation of oxidative stress by the anti-aging hormone klotho. *J. Biol. Chem.* **280**, 38029–38034. <https://doi.org/10.1074/jbc.M509039200> (2005).
- Chen, G. *et al.* alpha-Klotho is a non-enzymatic molecular scaffold for FGF23 hormone signalling. *Nature* **553**, 461–466. <https://doi.org/10.1038/nature25451> (2018).
- Abraham, C. R. & Li, A. Aging-suppressor Klotho: Prospects in diagnostics and therapeutics. *Ageing Res. Rev.* **82**, 101766. <https://doi.org/10.1016/j.arr.2022.101766> (2022).
- Nabeshima, Y. & Imura, H. Alpha-Klotho: A regulator that integrates calcium homeostasis. *Am. J. Nephrol.* **28**, 455–464. <https://doi.org/10.1159/000112824> (2008).
- Huang, C. L. Regulation of ion channels by secreted Klotho: Mechanisms and implications. *Kidney Int.* **77**, 855–860. <https://doi.org/10.1038/ki.2010.73> (2010).
- Tsujiikawa, H., Kurotaki, Y., Fujimori, T., Fukuda, K. & Nabeshima, Y. Klotho, a gene related to a syndrome resembling human premature aging, functions in a negative regulatory circuit of vitamin D endocrine system. *Mol. Endocrinol.* **17**, 2393–2403. <https://doi.org/10.1210/me.2003-0048> (2003).
- Forster, R. E. *et al.* Vitamin D receptor controls expression of the anti-aging klotho gene in mouse and human renal cells. *Biochem. Biophys. Res. Commun.* **414**, 557–562. <https://doi.org/10.1016/j.bbrc.2011.09.117> (2011).
- Richter, B. & Faul, C. FGF23 actions on target tissues-with and without klotho. *Front. Endocrinol.* **9**, 189. <https://doi.org/10.3389/fendo.2018.00189> (2018).
- Laszczyk, A. M. *et al.* FGF-23 deficiency impairs hippocampal-dependent cognitive function. *ENeuro*. <https://doi.org/10.1523/ENEURO.0469-18.2019> (2019).
- Liu, S. *et al.* Pathogenic role of Fgf23 in Hyp mice. *Am. J. Physiol. Endocrinol. Metab.* **291**, E38–E49. <https://doi.org/10.1152/ajpendo.00008.2006> (2006).
- Dubal, D. B. *et al.* Life extension factor klotho prevents mortality and enhances cognition in hAPP transgenic mice. *J. Neurosci.* **35**, 2358–2371. <https://doi.org/10.1523/JNEUROSCI.5791-12.2015> (2015).

21. Kurosu, H. *et al.* Suppression of aging in mice by the hormone Klotho. *Science* **309**, 1829–1833. <https://doi.org/10.1126/science.1112766> (2005).
22. Smith, R. C. *et al.* Circulating alphaKlotho influences phosphate handling by controlling FGF23 production. *J. Clin. Investig.* **122**, 4710–4715. <https://doi.org/10.1172/JCI64986> (2012).
23. Cha, S. K. *et al.* Regulation of renal outer medullary potassium channel and renal K(+) excretion by Klotho. *Mol. Pharmacol.* **76**, 38–46. <https://doi.org/10.1124/mol.109.055780> (2009).
24. Xiao, Z. *et al.* FGF23 expression is stimulated in transgenic alpha-Klotho longevity mouse model. *JCI Insight* **4**, 132820. <https://doi.org/10.1172/jci.insight.132820> (2019).
25. Xiao, X., Liu, X. & Jiao, B. Epigenetics: Recent advances and its role in the treatment of Alzheimer's disease. *Front. Neurol.* **11**, 538301. <https://doi.org/10.3389/fneur.2020.538301> (2020).
26. Komaba, H. *et al.* Klotho expression in osteocytes regulates bone metabolism and controls bone formation. *Kidney Int.* **92**, 599–611. <https://doi.org/10.1016/j.kint.2017.02.014> (2017).
27. Brownstein, C. A. *et al.* A translocation causing increased alpha-klotho level results in hypophosphatemic rickets and hyperparathyroidism. *Proc. Natl. Acad. Sci. U.S.A.* **105**, 3455–3460. <https://doi.org/10.1073/pnas.0712361105> (2008).
28. Sasaki, M. *et al.* Altered distribution of bone matrix proteins and defective bone mineralization in klotho-deficient mice. *Bone* **57**, 206–219. <https://doi.org/10.1016/j.bone.2013.08.008> (2013).
29. Toan, N. K., Tai, N. C., Kim, S. A. & Ahn, S. G. Soluble Klotho regulates bone differentiation by upregulating expression of the transcription factor EGR-1. *FEBS Lett.* **594**, 290–300. <https://doi.org/10.1002/1873-3468.13613> (2020).
30. Piedra, J. *et al.* Development of a rapid, robust, and universal picogreen-based method to titer adeno-associated vectors. *Hum. Gene Ther. Methods* **26**, 35–42. <https://doi.org/10.1089/hgtb.2014.120> (2015).

Acknowledgements

We thank Dr. Miquel Punset and Dr. Meritxell Molmeneu, at the Biomaterials, Biomechanics and Tissue Engineering Group, Department of Materials Science and Metallurgy (Technical University of Catalonia, UPC), for their support during the three-point bending test experiment.

Author contributions

J.R., C.S., A.B., F.V., and M.C. designed research. J.R. and C.S., performed research. J.R., C.S., J.E., S.V., C.R.A., A.B., F.V., and M.C. analyzed and interpreted the data. J.R. and M.C. wrote the paper. M.C. is the corresponding author. All authors read and approved the final manuscript.

Funding

This project was supported by the Ministerio Ciencia Innovación, Retos Sociedad (PID2019-104034RB-I00), the Ministerio de Economía, Industria y Competitividad (PID2020-116735RB-I00), the “Redes de Investigación Cooperativa Orientadas a Resultados en Salud” (RICORS) of the Carlos III Institute of Health (RD21/0017/0008). J.R., S.V. and J.E are recipients of fellowships by the Generalitat de Catalunya (2018FI_B00657), (2020FI_B100054) and (2020FI_SDUR0037).

Competing interests

Portions of this work are the subject of a patent application held by the Universitat Autònoma de Barcelona (UAB, Spain); the Universitat de Barcelona (UB, Spain); the Institutio Catalana de Recerca i Estudis Avançats (ICREA, Spain); and the Vall d'Hebron Institute of Research (VHIR, Spain). J.R., A.B., and M.C. are included in this patent application. C.R.A. is the co-founder of Klogenix, a company that is seeking to develop Klotho-boosting therapeutics. No other authors possess a conflict of interest.

Additional information

Correspondence and requests for materials should be addressed to M.C.

Reprints and permissions information is available at www.nature.com/reprints.

Publisher's note Springer Nature remains neutral with regard to jurisdictional claims in published maps and institutional affiliations.



Open Access This article is licensed under a Creative Commons Attribution 4.0 International License, which permits use, sharing, adaptation, distribution and reproduction in any medium or format, as long as you give appropriate credit to the original author(s) and the source, provide a link to the Creative Commons licence, and indicate if changes were made. The images or other third party material in this article are included in the article's Creative Commons licence, unless indicated otherwise in a credit line to the material. If material is not included in the article's Creative Commons licence and your intended use is not permitted by statutory regulation or exceeds the permitted use, you will need to obtain permission directly from the copyright holder. To view a copy of this licence, visit <http://creativecommons.org/licenses/by/4.0/>.

© The Author(s) 2023